Effect of different precursors on CVD growth of molybdenum disulfide

Aditya Singh*, Monika Moun, and Rajendra Singh

Department of Physics, Indian Institute of Technology Delhi, New Delhi 110016, India

* adityasingh27993@gmail.com

Abstract

Control over thickness, size, and area of chemical vapor deposition (CVD) grown molybdenum

disulfide (MoS2) flakes is crucial for device application. Herein, we report a quantitative

comparison of CVD synthesis of MoS2 on SiO2/Si substrate using three different precursors viz.,

molybdenum trioxide (MoO₃), ammonium heptamolybdate (AHM), and tellurium (Te). A three-

step chemical reaction mechanism of evolution of MoS₂ from MoO₃ micro-crystals is proposed

for MoO₃ precursor. Furthermore, a strategy based on growth temperature and ratio of amount of

precursors is developed to systematically control thickness and area of MoS2 flakes. Our findings

show that for large-sized crystalline monolayer MoS₂ flakes, MoO₃ is a better choice than AHM

and Te-assisted synthesis. Moreover, Te as growth promoter, can lower down growth temperature

by ~250°C. This study can be further used to fabricate MoS₂ based high-performance electronic

devices such as photodetectors, thin film transistors, and sensors.

Keywords: Chemical vapor deposition; MoS2; MoO3; tellurium; ammonium heptamolybdate;

Raman.

1. Introduction

Two-dimensional (2D) materials, namely graphene, black phosphorus, hexagonal boron nitride,

and transition metal dichalcogenides (TMDCs) have gained tremendous attention due to their

unique optical, electrical, and mechanical properties[1,2]. Graphene being a zero bandgap 2D-

1

material, has limited applications in opto-electronics devices[3]. Possible ideal materials for replacement of graphene in future are TMDCs, depicted by TX2, where T and X are transition metal (Mo, W, Nb, Ti etc.) and chalcogen (S, Se, and Te), respectively e.g., MoS2, MoSe2, and MoTe2 etc[1]. In most of the semiconducting TMDCs, a transition from an indirect bandgap to a direct bandgap has been observed as number of layers decrease due to the quantum confinement effect[2]. Molybdenum disulphide (MoS2), a member of TMDCs family, has been widely explored due to tunability of bandgap (1.3 eV in bulk and 1.8 eV in monolayer)[4], high elastic modulus (~170 N/m)[5], high on/off ratio (~108)[6], high carrier mobility (40-480 cm2/V-s)[7], and lack of short channel effect[7], which makes it appropriate for application in flexible devices[5,7], high performance field-effect-transistors (FETs)[7,8], photodetectors[9,10] and gas sensors[11] etc.

Inter-layer strong covalent and intra-layer weak van der Waals bonding makes peeling of MoS₂ layers easier[1,2]. Till now, various methods have been developed to grow layered MoS₂ such as mechanical exfoliation (scotch tape) [7,12], physical vapor deposition (sputtering and pulsed laser deposition)[13], one-step CVD (direct reaction of S and Mo source)[13], and two-step CVD (sulfurization of pre-deposited Mo film)[14,15] etc. Mechanical exfoliation method was employed to obtain high-quality layered MoS₂ films but this approach limits its industrial growth and commercially viable device applications because of low yield and small size MoS₂ films/flakes[16,17]. Furthermore, the hydrothermal method was also employed to synthesize MoS₂ but failed due to the same limitations as of exfoliation[1,18,19]. Highly crystalline homogeneous monolayer MoS₂ with high yield and low cost having excellent electrical and optical properties is desirable. So, special attention has been given to CVD as it has a greater possibility to grow large area high-quality uniform mono- and few-layer MoS₂ with low manufacturing costs[20–22].

CVD growth of MoS₂ could be achieved by different Mo source materials such as molybdenum trioxide (MoO₃) powder[19,23–25], Mo film[26], ammonium heptamolybdate[21,27], gas source of Mo(CO)₆[20,23,27], and MoCl₅[20,23]. Zhan et al. [28] reported the growth of MoS₂ film on silicon dioxide (SiO₂) substrate by sulfurization of Mo metal film in a two-step CVD process but this approach resulted in a lack of crystallinity and poor electrical properties of MoS₂ films[29]. In a single-step process, Mo metal film was replaced by Mo sources such as MoO₃ powder, AHM or MoCl₅. MoS₂ flakes grown by MoCl₅ have superior uniformity and good transport properties but MoCl₅ being toxic can make growth hazardous[29]. For MoS₂ growth on the SiO₂/Si substrate, MoO₃ and S precursors have been dominantly used because of preferential highly crystalline monolayer MoS₂ having quite good electrical and optical properties at the wafer scale[30]. Cain et al. [31] proposed the mechanism for the MoS₂ nucleation, growth, and grain boundary formation to study systematically, and prepare large area, single- and few-layered TMDCs films. Gong et al. [32] suggested that use of Te can reduce the growth temperature of MoS₂, and Tao et al.[21] developed low-cost CVD method to grow centimetre size highly crystalline MoS₂ films by ammonium molybdate as Mo source precursor.

Our present work focuses on the effect of different Mo precursors (MoO₃ and AHM) on the shape, size, and crystallinity of monolayer (1L), bilayer (2L), and multilayer (bulk) MoS₂ flakes on SiO₂/Si substrate. Also, we used Te as growth intermediate along with MoO₃ to reduce growth temperature by ~250°C. It was observed that choice of precursors influences the geometry, crystallinity, and surface morphology of as-grown MoS₂ flakes.

2. Experimental

Single zone atmospheric pressure mini CVD (APCVD) tube system (MTI Corporation, OTF-1200X S50-2F) was used for the growth of 1L- and few-layer MoS₂ using different precursors such as sulfur (S) powder (99.98%, Sigma-Aldrich, 414980), MoO₃ powder (99.97%, Sigma-Aldrich, 203815), AHM [(NH4)6M07O24· 4H2O)] (99.98%, Sigma-Aldrich, 431346), and Te powder (99.997%, Sigma-Aldrich, 264865) on Si (001) n-type substrate covered with thermally grown 285 nm thick SiO₂ layer. The precursors and the substrates were placed in a 1.97 inch diameter and 17.7 inch long quartz tube, which was surrounded by the furnace (Fig. 1a). We did not perform any pre-growth treatment, such as seeded growth, use of molecular sieves or any step edges that may have adverse effects on electrical properties of flakes[21]. The substrates were cleaned with acetone followed by IPA and DI water, and placed face down on the top of boat shape quartz crucible (5.5 cm \times 2 cm \times 0.5 cm). Mo source was placed inside quartz boat under face down SiO₂/Si substrate at hottest zone (700-950°C) of the tube, and S powder was kept 16 cm away from MoO3 at a low-temperature gradient of the quartz tube. After both precursors and substrates were loaded into the tube, ~60 ml/min of argon (Ar) gas (~99%, Sigma Gases), controlled by mass flow controller, was introduced into the tube to purge the system. After all these processes, the furnace was started at a ramp rate of 10°C/min. Fig. 1b represents the CVD temperature-time graph for the temperature of Mo source versus time. At 300°C, the temperature was kept constant for 5 min so that all contaminants, pre-occupied precursors, moisture, and dust can be swept out by Ar gas flow. Melting and vaporisation of S were started at 600°C and 900°C (temperature at the centre of the tube), respectively, and the temperature was kept constant at 900°C for 20 min. Vaporised S particles were carried by Ar gas over the substrate where it reacted with vaporised MoO₃ particles, and formed different shape few- and 1L-MoS₂ flakes. The system was cooled down to room temperature, and byproducts were carried by continuous Ar gas flow.

Fig. 1c shows image of as-grown MoS2 sample on SiO2/Si substrate showing large area growth.

Blue boxes represent regions of grown MoS2 flakes while white boxes show MoO2 and/or MoOS2

grown regions.

Optical microscopy (OM) images of as-grown MoS₂ flakes of different shapes (triangles, truncated triangles, hexagons, bowtie, pine leaves, and stars) on SiO₂/Si substrate were captured by Nikon Eclipse LV100 microscope. Both Raman spectroscopy and photoluminescence measurements were carried out at room temperature by Renishaw-inVia-confocal-Raman microscope-6260 with 532 nm laser line and 1800 lines/mm grating on as-grown MoS₂ flakes to observe fundamental modes of MoS₂ (E_{12g} and A_{1g})[33] and their bandgaps, respectively. Layer numbers of crystalline MoS₂ flakes and its surface roughness were determined by atomic force microscopy (Bruker, Dimension Icon) in tapping mode with Si tip. To observe the surface morphology and elemental contrast, field emission scanning electron microscopy (FESEM) was carried out by FESEM-Zeiss

3. Results and discussion

microscope in back scattering mode.

Uniform large size high quality MoS₂ flakes on SiO₂/Si substrate were grown by CVD using three different methods as illustrated below.

3.1. Growth of MoS₂ using S and MoO₃

MoS₂ thin layers were grown using MoO₃ and S powder by systematically optimising the growth parameters such as amount of precursors and growth temperature. Initially, the S content (20-500 mg) was optimized with the constant loading of 20 mg MoO₃. Considering the concept of mole, 1

mg of S (atomic weight ~32) contains ~1.88 × 1019 atoms while 1 mg of MoO3 (atomic weight ~144) contains ~4.18 × 10₁₈ molecules. At S=20 mg (S to MoO₃ particles ratio ~5:1), T= 700°C, and at vacuum (~5 torr), no proper deposition was obtained. Inside the quartz tube, S vapor particles are in the downstream flow, and atomically, they need to travel very large distance (16 cm) to reach over the SiO₂/Si substrate where they will react with MoO₃ vapor particles. Most of S vapor particles go unreacted and flushed out of the outlet. So, we need to increase the amount of S in order to increase the reaction possibility. When the S amount was doubled to 40 mg (S to MoO₃ particles ratio ~10:1) that resulted in formation of clusters and grains of oxy-particles of MoO₃ (MoO₂) uniformly all over the substrate as shown in Fig. 2a. Again when the amount of S was further increased to 80 mg (S to MoO₃ particles ratio ~18:1) and temperature to 800°C at atmospheric pressure, small-sized (~3 µm) oxy-phase of MoS2 (MoOS2) flakes were obtained (Fig. 2b). Insufficient supply of S caused the formation of MoO₂ or MoOS₂, and these oxy-phases acted as nucleation centres for MoS₂ growth[25]. When amount of MoO₃ was decreased from 20 mg to 15 mg (S to MoO₃ particles ratio ~30:1), large triangles (~20-80 μm) of 1L-MoS₂ on the large area (~3 mm × 4 mm) were observed (Fig. 2c). Fig. 2c shows the growth of a few 2L-MoS₂ triangular flakes (~2 µm) over 1L-MoS2 flakes. Lateral growth of 1L-MoS2 flakes over SiO2/Si substrate was caused by lateral strong covalent bonding while growth of small-sized 2L-MoS2 flakes over 1L-MoS₂ was caused by vertical weak van der Waals epitaxy[34]. Bright triangular flake at the bottom right of Fig. 2c shows a multilayer growth of MoS₂. So, at more S vapor particles than MoO₃ (S to MoO₃ particles ratio ~30:1), crystalline MoS₂ flakes can be easily grown. Fig. 2d-i represent FESEM images (in back-scattering mode) of as-grown MoS₂ flakes synthesised by S and MoO₃ precursors representing the evolution of MoS₂ from MoO₃ oxy-phase (MoO₂) to highly crystalline uniform large-sized triangular 1L-MoS2 flakes. These FESEM images clearly show the optical and

compositional contrast of flakes with respect to SiO₂/Si substrate. **Fig. 2d,e** represent FESEM images of MoO₂ and MoOS₂ flakes corresponding to OM images 2(a) and(b), respectively. **Fig. 2f** shows rectangular bulk MoS₂ micro-crystals deposited at the boundary of contact between substrate and quartz boat. **Fig. 2g** depicts polycrystalline continuous bulk MoS₂ growth along with few single crystalline MoS₂ triangular flakes, and **Fig. 2h** shows a few hexagonal flakes along with truncated triangles which may be considered as the basic building block of triangular MoS₂ flakes[19]. In **Fig. 2i**, MoS₂ triangular flakes are very sharp and have uniform surface morphology, depicting very high single crystallinity.

Sulfurization of MoO₃ shows the transformation of MoO₃ to MoS₂ involving three intermediate steps[15]. At first, MoO₃ powder thermally evaporates at ~700°C, reduced using S, and recondense to obtain MoO₂ micro-crystals where each removed oxygen atom partakes in forming SO₂. A possible chemical reaction is:

$$2\text{MoO}_3 + \text{S} \rightarrow 2\text{MoO}_2 + \text{SO}_2 \uparrow \tag{1}$$

In the second step, MoO₂ micro crystals again sulfurize under appropriate conditions at ~800°C to form MoOS₂ phase.

$$2\text{MoO}_2 + 3\text{S} \rightarrow 2\text{MoOS}_2 + \text{SO}_2 \uparrow \tag{2}$$

And finally, MoOS₂ crystals further sulfurize layer-by-layer at ~900°C to obtain 2D-MoS₂ crystals:

$$2\text{MoOS}_2 + \text{S} \rightarrow 2\text{MoS}_2 + \text{SO}_2 \uparrow \tag{3}$$

3.2. Growth of MoS2 using S and AHM

Tao et al.[21] suggested that Mo vapor precursors, generated from AHM [(NH₄)6Mo₇O₂₄· 4H₂O)] instead of MoO₃, in low diffusion rate enable growth of low nuclei density which produce largesized crystalline MoS₂ film. So, in this case, MoO₃ powder was replaced by AHM. Amount of S precursor and Ar flow were kept fixed at 100 mg and 60 ml/min, respectively, whereas amount of AHM precursor and growth temperature were varied systematically. Initially, at AHM= 20 mg (S to AHM particles ratio ~193:1) and T= 900°C, round shape MoS₂ oxy-flakes (~1-10 μm) having a nucleation centre at mid of the flakes, were synthesised (Fig. 3a). Furthermore, to convert the oxy-phase round shape MoS₂ to triangular MoS₂ flakes, amount of AHM was decreased to 15 mg (S to AHM particles ratio ~257:1), and growth temperature increased to 950°C. High-quality largesized 1L-MoS₂ flakes (sky blue triangles, ~1-50 μm) along with bulk MoS₂ (bright triangles, ~1-20 μm) (**Fig. 3b**) were observed. When growth temperature was further increased to 1000°C, uniform growth of high-quality 1L- and few bulk MoS₂ triangles (~20-80 μm) over a large area of the substrate (~5 mm × 10 mm) were obtained (Fig. 3c). Fig. 3b,c correspond to high-quality MoS₂ flakes grown over a large area obtained at nearly same growth conditions, which implicate high repeatability of the method in the temperature range 950-1000°C. Fig. 3d-f correspond to FESEM images of MoOS2 with few MoS2 flakes, bulk and 1L-MoS2 triangular flakes, and large-sized crystalline 1L-MoS₂ flakes, respectively. At the high temperature (900-1000°C), pyrolysis occurs that causes molecular breakdown of AHM. Possible pyrolysis reaction of AHM is as follows [21]:

$$(NH_4)_6M_{O7}O_{24} \cdot 4H_2O \rightarrow 7M_0O_3 + 6NH_3 \uparrow + 7H_2O \uparrow$$
(4)

MoO₃ vapor particle reacts with S vapors while ammonia gas (NH₃) and water vapors (H₂O) are flushed out. A very high number of S atoms supply (S to AHM particles ratio ~257:1) was required

to synthesise MoS₂, so that S atoms can easily react with MoO₃ molecules obtained from breakdown of AHM. Further, growth mechanism could be considered similar to MoO₃ which produce MoS₂ in three aforementioned steps.

3.3. Tellurium assisted growth of MoS₂

For large scale industrial synthesis of MoS2, there is a pressing need to lower down growth temperature. Gong et al.[32] reduced the growth temperature of MoS2 by 200°C by using Te as growth intermediate in two zone CVD furnace. In our work, CVD synthesis of Te-assisted MoS2 crystalline triangular flakes on SiO2/Si substrate at atmospheric pressure were optimised at a constant loading of source precursors at Te= 15 mg, S= 100 mg, and MoO₃= 15 mg (S to MoO₃ to Te particles ratio ~30:1:1.13) with different growth temperature. A mixture of MoO₃ and Te powder was loaded in quartz tube underneath the SiO2/Si substrate (face-down manner). At a temperature of 650°C, triangular star shape bulk MoS₂ flakes (bright blue triangles, ~10-30 µm) were grown over the island of 1L-MoS₂ flakes (purple triangles, ~20-70 μm) (Fig. 4a). Fig. 4b shows the OM image of crystalline 1L-MoS₂ synthesised at 700°C with lateral size up to 50 µm. Fig. 4c represents very large size (~50-150 μm) highly crystalline uniformly grown pine shape triangular bulk MoS₂ flakes over the large area (~5 mm × 6 mm). Furthermore, Fig. 4d-f are FESEM images corresponding to Fig. 4a-c. Initially, at temperature lower than 650°C, small fraction of MoO₃ powder dissolve in molten Te which make unstable ternary alloy MoS_xTe_{2-x} under continuous flow of S atoms [32,35]. This unstable alloy acts as a reaction intermediate which at higher temperature result in 2D-MoS₂ flakes, and byproducts are flushed out by Ar gas[32,34]. Without the use of Te powder, MoS₂ growth temperature was 900°C. Hence, introduction of Te accelerates growth and lower down MoS₂ growth temperature by ~250°C which could be useful for large scale MoS₂ growth[34].

4. Raman analysis

Raman spectroscopy was carried out on as-grown MoS₂ flakes. There are first-order four Raman-active vibrational modes (E_{22g}, E_{1g}, E_{12g}, and A_{1g}) in MoS₂[33]. E_{12g} mode corresponds to in-plane vibration of two S atoms in opposite direction to Mo atom, and A_{1g} mode represents out-of-plane vibration of two S atoms in opposite direction while Mo atom remains at rest[33,36]. E_{12g} and A_{1g} as fundamental first-order Raman modes of MoS₂ were observed while rest of the two modes were undetectable due to the limited rejection of the Rayleigh scattered radiation in our Renishaw-inViaconfocal-Raman microscope-6260.

Initially, we observed the oxy-phase of MoO₃ (MoO₂) that resulted in many Raman peaks around at 128, 206, 230, 352, 367, 466, 498, 571, 592, and 746 cm-1 (**Fig. 5a**). These Raman peaks of MoO₂ match well with reported results[37]. Raman spectra of MoO₂ was taken from the same sample whose OM and SEM images are shown in **Fig. 2a,d**, respectively. Furthermore, an increased amount of S resulted in the oxy-phase of MoS₂ (MoOS₂) whose Raman peaks are observed at around 127, 206, 231, 367, 474, and 499 cm-1 for MoOS₂[25], and 384 cm-1 and 409 cm-1 for bulk MoS₂ (**Fig. 5b**). Raman spectra of MoOS₂ was taken from the same sample whose OM and SEM images are shown in **Fig. 2b,e**, respectively. Peak frequency difference (Δ k) in these E12g and A1g mode is closely related to a number of layers[33,38]. For a given λ , the difference between E12g and A1g modes decreases with decreasing thickness of MoS₂. It has been reported that Δ k of E12g and A1g modes for monolayer is < 21 cm-1, ~21-22 cm-1 for bilayer, and Δ k > 25 cm-1 for bulk MoS₂[32,39]. **Fig. 5c** represents Raman spectra of crystalline 1L, 2L, and bulk MoS₂

synthesised using MoO₃ and S powder. For 1L-MoS₂, E_{12g} and A_{1g} Raman modes observed at 384 and 404.2 cm-1 and their Δk for these modes is 20.2 cm-1 which corresponds to monolayer MoS2 (Fig. 5c). For 2L-MoS₂, E_{12g} and A_{1g} mode were observed at 383.3 and 404.5 cm-1, and for bulk MoS₂, modes are observed at 382.7 and 409.4 cm₋₁, respectively (**Fig. 5c**). As the layer numbers of MoS₂ increase, A_{1g} Raman mode shows blue shifts while E_{12g} mode shows red shifts. Blue shifts of A_{1g} mode can be attributed to increased restoring force because of interlayer van der Waals interaction between layers of MoS2. Furthermore, this restoring force consideration does not predict the behaviour of E_{12g} mode (in-plane vibration) so, it is assumed that this anomaly is caused by stacking induced structural change and/or long-range coulombic interaction[33]. Greater intensity of A_{1g} mode than E_{12g} for bulk MoS₂ shows stronger out-of-plane vibration of MoS₂ molecule while comparatively equal intensities of A_{1g} and E_{12g} modes represents weak coupling between electronic transition at K-point[38] (Fig. 5c). Raman spectra of CVD MoS₂ synthesised by AHM powder and Te-assisted are shown in Fig. 5d,e, respectively. Raman intensity of A_{1g} mode is considerably higher than the E_{12g} mode for 1L, 2L, and bulk MoS₂ for AHM powder and Te-assisted CVD MoS₂ depicting strong out of plane vibration of MoS₂ (Fig. 5d,e).

5. Photoluminescence analysis

Photoluminescence (PL) spectroscopy was carried out with 532 nm laser line on 1L-MoS₂ triangular flakes to determine the bandgap. PL spectra of MoS₂ triangular flakes grown via a different combination of precursors are shown in **Fig. 5f**. PL spectrum (1), (2), and (3) correspond to MoS₂ flakes synthesised by MoO₃, AHM, and Te-assisted, respectively. PL spectrum (1) shows A exciton peak at 668 nm (1.856 eV) and B exciton peak around 620 nm (2.0 eV). Spin-orbit coupling causes splitting of valence band which leads to A and B excitonic transitions [40,41]. These two A and B excitons are generated because of radiative recombination of electrons and

holes in a neutral exciton at the Brillouin zone K-point[40]. The energy of valence band splitting is 144 meV (2.0-1.856 eV), and A exciton transition occur from top of valence band while B exciton from the bottom of the valence band. PL spectrum (2) and (3) correspond to 1L-MoS₂ flakes synthesised by AHM and Te-assisted, respectively. A and B excitons position were observed at 666 nm (1.861 eV) and 622 nm (1.994 eV), respectively for AHM precursor and at 680 nm (1.823 eV) and 634 nm (1.956 eV) for Te-assisted growth. Valence band splitting for both AHM precursor and Te assisted growth was observed at 133 meV.

6. Morphological study of as-synthesised MoS2 flakes

Tapping mode atomic force microscopy (AFM) was carried out to see surface morphology and to determine the thickness of MoS₂ flakes. Fig. 6a-c are AFM height images corresponding to CVD synthesised MoS₂ flakes grown by precursors MoO₃, AHM, and Te-assisted, respectively. AFM height images are taken from the same samples for which OM images are shown in Fig. 2c, 3c, and 4c, and SEM images are shown in Fig. 2i, 3f and 4f. AFM height profiles of corresponding AFM images are inserted in respective Figures. In **Fig. 6a**, AFM height image shows the thickness of 1L-MoS₂ to be 0.88 nm (with high uniformity of surface) nearly similar to the theoretical value of 0.62 nm[42]. While CVD MoS₂ synthesised by AHM and Te-assisted give monolayer thickness to be 1.05 nm and 1.25 nm, respectively (**Fig. 6b,c**). Relatively higher value of the thickness of 1L-MoS₂ are regarded as SiO₂/Si substrate has some absorbents on its surface[33]. Comparing surface topography of Fig. 6a-c, it is observed that triangular flake of Fig. 6b has some 2L-MoS₂ grown over 1L-MoS₂ flake, and corners of the 1L-MoS₂ triangle are truncated. Similarly, the triangular 1L-MoS2 flakes are shown in **Fig. 6c** has irregular sides, and bulk MoS2 triangles (bright triangles) of very small size are grown over 1L-MoS₂ flake. Analysing the surface roughness, homogeneity, and uniformity of these flakes make it clear that the morphology of MoS₂ flakes

synthesised by MoO₃ precursors is smoother with better uniformity as compared to AHM and Teassisted growth. AFM height images are taken from the same samples for which optical images are shown in **Fig. 2d,g** and **i**, and SEM images are shown in **Fig. 3f, 4c** and **4f**.

4. Conclusions

Effect of different precursors on CVD growth of MoS2 on SiO2/Si substrate was studied by changing growth temperature and precursors ratio. Highly crystalline large-sized 1L-MoS2 flakes were obtained at S to MoO3 particles ratio of ~30:1. With the introduction of Te, MoS2 growth temperature is lowered down by ~250°C that could be useful in low-temperature large scale growth of MoS2 flakes. For large-sized crystalline 1L-MoS2 flakes, MoO3 powder is a better choice, and for large area bulk MoS2, both AHM powder and Te-assisted synthesis both can be chosen. MoS2 flakes grown by MoO3 and S precursors shows better uniformity, crystallinity, and reproducibility as compared to AHM and Te-assisted growth. Photoluminescence reveals that the energy of valence band splitting (144 meV) is higher for MoO3 than AHM and Te-assisted 1L-MoS2 (133 meV) synthesis. With the help of Raman spectroscopy, we propose three-step chemical reaction of evolution of MoS2 from vapor phase MoO3 micro-particles. This study can be further used to fabricate MoS2 based high-performance electronic devices such as sensors, thin film transistors, and photodetectors.

Acknowledgements

The authors gratefully acknowledge the Nanoscale Research Facility (NRF) and FIST-UFO scheme at the Indian Institute of Technology Delhi for providing AFM characterizations, and Raman and photoluminescence measurements, respectively. Aditya Singh would like to thank the University Grants Commission (UGC), India for providing research fellowship.

References

- [1] Q.H. Wang, K. Kalantar-Zadeh, A. Kis, J.N. Coleman, M.S. Strano, Electronics and optoelectronics of two-dimensional transition metal dichalcogenides, Nat. Nanotechnol. 7 (2012) 699.
- [2] M. Ye, D. Winslow, D. Zhang, R. Pandey, Y.K. Yap, Recent advancement on the optical properties of two-dimensional molybdenum disulfide (MoS₂) thin films, in: Photonics, Multidisciplinary Digital Publishing Institute, 2015: pp. 288–307.
- [3] A.H. Castro Neto, F. Guinea, N.M.R. Peres, K.S. Novoselov, A.K. Geim, The electronic properties of graphene, Rev. Mod. Phys. 81 (2009) 109–162. doi:10.1103/RevModPhys.81.109.
- [4] A. Kuc, N. Zibouche, T. Heine, Influence of quantum confinement on the electronic structure of the transition metal sulfide TS₂, Phys. Rev. B. 83 (2011) 245213. doi:10.1103/PhysRevB.83.245213.
- [5] K. Liu, Q. Yan, M. Chen, W. Fan, Y. Sun, J. Suh, D. Fu, S. Lee, J. Zhou, S. Tongay, J. Ji, J.B. Neaton, J. Wu, Elastic Properties of Chemical-Vapor-Deposited Monolayer MoS₂, WS₂, and Their Bilayer Heterostructures, Nano Lett. 14 (2014) 5097–5103. doi:10.1021/nl501793a.
- [6] R. Kitaura, Y. Miyata, R. Xiang, J. Hone, J. Kong, R.S. Ruoff, S. Maruyama, Chemical Vapor Deposition Growth of Graphene and Related Materials, J. Phys. Soc. Jpn. 84 (2015) 121013. doi:10.7566/JPSJ.84.121013.
- [7] P.-Z. Shao, H.-M. Zhao, H.-W. Cao, X.-F. Wang, Y. Pang, Y.-X. Li, N.-Q. Deng, J. Zhang, G.-Y. Zhang, Y. Yang, S. Zhang, T.-L. Ren, Enhancement of carrier mobility in MoS₂ field effect transistors by a SiO2 protective layer, Appl. Phys. Lett. 108 (2016) 203105. doi:10.1063/1.4950850.
- [8] H. Peelaers, C.G. Van de Walle, Effects of strain on band structure and effective masses in MoS2, Phys. Rev. B. 86 (2012) 241401. doi:10.1103/PhysRevB.86.241401.
- [9] M. Moun, M. Kumar, M. Garg, R. Pathak, R. Singh, Understanding of MoS₂/GaN Heterojunction Diode and its Photodetection Properties, Sci. Rep. 8 (2018). doi:10.1038/s41598-018-30237-8.
- [10] O. Lopez-Sanchez, D. Lembke, M. Kayci, A. Radenovic, A. Kis, Ultrasensitive photodetectors based on monolayer MoS₂, Nat. Nanotechnol. 8 (2013) 497–501. doi:10.1038/nnano.2013.100.
- [11] A. Shokri, N. Salami, Gas sensor based on MoS₂ monolayer, Sens. Actuators B Chem. 236 (2016) 378–385. doi:10.1016/j.snb.2016.06.033.
- [12] S. Zheng, J. So, F. Liu, Z. Liu, N. Zheludev, H.J. Fan, Efficient cathodoluminescence of monolayer transitional metal dichalcogenides in a van der Waals heterostructure, Nano Lett. 17 (2017) 6475–6480. doi:10.1021/acs.nanolett.7b03585.
- [13] S.H. Baek, Y. Choi, W. Choi, Large-Area Growth of Uniform Single-Layer MoS₂ Thin Films by Chemical Vapor Deposition, Nanoscale Res. Lett. 10 (2015) 388. doi:10.1186/s11671-015-1094-x.
- [14] K.M. McCreary, A.T. Hanbicki, J.T. Robinson, E. Cobas, J.C. Culbertson, A.L. Friedman, G.G. Jernigan, B.T. Jonker, Large-Area Synthesis of Continuous and Uniform MoS₂ Monolayer

- Films on Graphene, Adv. Funct. Mater. 24 (2014) 6449–6454. doi:10.1002/adfm.201401511.
- [15] I. Bilgin, F. Liu, A. Vargas, A. Winchester, M.K.L. Man, M. Upmanyu, K.M. Dani, G. Gupta, S. Talapatra, A.D. Mohite, S. Kar, Chemical Vapor Deposition Synthesized Atomically Thin Molybdenum Disulfide with Optoelectronic-Grade Crystalline Quality, ACS Nano. 9 (2015) 8822–8832. doi:10.1021/acsnano.5b02019.
- [16] K.S. Novoselov, A. Mishchenko, A. Carvalho, A.H.C. Neto, 2D materials and van der Waals heterostructures, Science. 353 (2016) aac9439. doi:10.1126/science.aac9439.
- [17] M. O'Brien, N. McEvoy, D. Hanlon, T. Hallam, J.N. Coleman, G.S. Duesberg, Mapping of Low-Frequency Raman Modes in CVD-Grown Transition Metal Dichalcogenides: Layer Number, Stacking Orientation and Resonant Effects, Sci. Rep. 6 (2016) 19476. doi:10.1038/srep19476.
- [18] Y.-H. Lee, X.-Q. Zhang, W. Zhang, M.-T. Chang, C.-T. Lin, K.-D. Chang, Y.-C. Yu, J.T.-W. Wang, C.-S. Chang, L.-J. Li, T.-W. Lin, Synthesis of Large-Area MoS₂ Atomic Layers with Chemical Vapor Deposition, Adv. Mater. 24 (2012) 2320–2325. doi:10.1002/adma.201104798.
- [19] S. Wang, Y. Rong, Y. Fan, M. Pacios, H. Bhaskaran, K. He, J.H. Warner, Shape Evolution of Monolayer MoS₂ Crystals Grown by Chemical Vapor Deposition, Chem. Mater. 26 (2014) 6371–6379. doi:10.1021/cm5025662.
- [20] Y. Xie, Z. Wang, Y. Zhan, P. Zhang, R. Wu, T. Jiang, S. Wu, H. Wang, Y. Zhao, Tang Nan, X. Ma, Controllable growth of monolayer MoS₂ by chemical vapor deposition via close MoO₂ precursor for electrical and optical applications, Nanotechnology. 28 (2017) 084001. doi:10.1088/1361-6528/aa5439.
- [21] L. Tao, K. Chen, Z. Chen, W. Chen, X. Gui, H. Chen, X. Li, J.-B. Xu, Centimeter-Scale CVD Growth of Highly Crystalline Single-Layer MoS₂ Film with Spatial Homogeneity and the Visualization of Grain Boundaries, ACS Appl. Mater. Interfaces. 9 (2017) 12073–12081. doi:10.1021/acsami.7b00420.
- [22] A. Özden, F. Ay, C. Sevik, N.K. Perkgöz, CVD growth of monolayer MoS₂: Role of growth zone configuration and precursors ratio, Jpn. J. Appl. Phys. 56 (2017) 06GG05. doi:10.7567/JJAP.56.06GG05.
- [23] S. Wang, M. Pacios, H. Bhaskaran, J.H. Warner, Substrate control for large area continuous films of monolayer MoS₂ by atmospheric pressure chemical vapor deposition, Nanotechnology. 27 (2016) 085604. doi:10.1088/0957-4484/27/8/085604.
- [24] B.M. Bersch, S.M. Eichfeld, Y.-C. Lin, K. Zhang, G.R. Bhimanapati, A.F. Piasecki, M.L. III, J.A. Robinson, Selective-area growth and controlled substrate coupling of transition metal dichalcogenides, 2D Mater. 4 (2017) 025083. doi:10.1088/2053-1583/aa6beb.
- [25] V. Senthilkumar, L.C. Tam, Y.S. Kim, Y. Sim, M.-J. Seong, J.I. Jang, Direct vapor phase growth process and robust photoluminescence properties of large area MoS₂ layers, Nano Res. 7 (2014) 1759–1768. doi:10.1007/s12274-014-0535-7.
- [26] Y. Shi, H. Li, L.-J. Li, Recent advances in controlled synthesis of two-dimensional transition metal dichalcogenides via vapour deposition techniques, Chem. Soc. Rev. 44 (2015) 2744–2756. doi:10.1039/C4CS00256C.

- [27] Z. Cai, B. Liu, X. Zou, H.-M. Cheng, Chemical Vapor Deposition Growth and Applications of Two-Dimensional Materials and Their Heterostructures, Chem. Rev. 118 (2018) 6091–6133. doi:10.1021/acs.chemrev.7b00536.
- [28] Y. Zhan, Z. Liu, S. Najmaei, P.M. Ajayan, J. Lou, Large-Area Vapor-Phase Growth and Characterization of MoS₂ Atomic Layers on a SiO₂ Substrate, Small. 8 (2012) 966–971. doi:10.1002/smll.201102654.
- [29] P. Gnanasekar, D. Periyanagounder, A. Nallathambi, S. Subramani, M. Palanisamy, J. Kulandaivel, Promoter-free synthesis of monolayer MoS2 by chemical vapour deposition, CrystEngComm. 20 (2018) 4249–4257. doi:10.1039/C8CE00576A.
- [30] Y.-H. Lee, L. Yu, H. Wang, W. Fang, X. Ling, Y. Shi, C.-T. Lin, J.-K. Huang, M.-T. Chang, C.-S. Chang, M. Dresselhaus, T. Palacios, L.-J. Li, J. Kong, Synthesis and Transfer of Single-Layer Transition Metal Disulfides on Diverse Surfaces, Nano Lett. 13 (2013) 1852–1857. doi:10.1021/nl400687n.
- [31] J.D. Cain, F. Shi, J. Wu, V.P. Dravid, Growth Mechanism of Transition Metal Dichalcogenide Monolayers: The Role of Self-Seeding Fullerene Nuclei, ACS Nano. 10 (2016) 5440–5445. doi:10.1021/acsnano.6b01705.
- [32] Y. Gong, Z. Lin, G. Ye, G. Shi, S. Feng, Y. Lei, A.L. Elías, N. Perea-Lopez, R. Vajtai, H. Terrones, Z. Liu, M. Terrones, P.M. Ajayan, Tellurium-Assisted Low-Temperature Synthesis of MoS₂ and WS₂ Monolayers, ACS Nano. 9 (2015) 11658–11666. doi:10.1021/acsnano.5b05594.
- [33] H. Li, Q. Zhang, C.C.R. Yap, B.K. Tay, T.H.T. Edwin, A. Olivier, D. Baillargeat, From Bulk to Monolayer MoS₂: Evolution of Raman Scattering, Adv. Funct. Mater. 22 (2012) 1385–1390. doi:10.1002/adfm.201102111.
- [34] Y. Gong, J. Lin, X. Wang, G. Shi, S. Lei, Z. Lin, X. Zou, G. Ye, R. Vajtai, B.I. Yakobson, H. Terrones, M. Terrones, B.K. Tay, J. Lou, S.T. Pantelides, Z. Liu, W. Zhou, P.M. Ajayan, Vertical and in-plane heterostructures from WS₂/MoS₂ monolayers, Nat. Mater. 13 (2014) 1135–1142. doi:10.1038/nmat4091.
- [35] J. Kang, S. Tongay, J. Li, J. Wu, Monolayer semiconducting transition metal dichalcogenide alloys: Stability and band bowing, J. Appl. Phys. 113 (2013) 143703. doi:10.1063/1.4799126.
- [36] K.-G. Zhou, F. Withers, Y. Cao, S. Hu, G. Yu, C. Casiraghi, Raman Modes of MoS₂ Used as Fingerprint of van der Waals Interactions in 2-D Crystal-Based Heterostructures, ACS Nano. 8 (2014) 9914–9924. doi:10.1021/nn5042703.
- [37] M.A. Camacho-López, L. Escobar-Alarcón, M. Picquart, R. Arroyo, G. Córdoba, E. Haro-Poniatowski, Micro-Raman study of the m-MoO₂ to a-MoO₃ transformation induced by cw-laser irradiation, Opt. Mater. 33 (2011) 480–484. doi:10.1016/j.optmat.2010.10.028.
- [38] C. Lee, H. Yan, L.E. Brus, T.F. Heinz, J. Hone, S. Ryu, Anomalous Lattice Vibrations of Single-and Few-Layer MoS₂, ACS Nano. 4 (2010) 2695–2700. doi:10.1021/nn1003937.
- [39] S.Y. Yang, G.W. Shim, S.-B. Seo, S.-Y. Choi, Effective shape-controlled growth of monolayer MoS_2 flakes by powder-based chemical vapor deposition, Nano Res. 10 (2017) 255–262. doi:10.1007/s12274-016-1284-6.
- [40] A. Splendiani, L. Sun, Y. Zhang, T. Li, J. Kim, C.-Y. Chim, G. Galli, F. Wang, Emerging Photoluminescence in Monolayer MoS₂, Nano Lett. 10 (2010) 1271–1275. doi:10.1021/nl903868w.

- [41] D. Kaplan, Y. Gong, K. Mills, V. Swaminathan, P.M. Ajayan, S. Shirodkar, E. Kaxiras, Excitation intensity dependence of photoluminescence from monolayers of MoS₂ and WS₂/MoS₂ heterostructures, 2D Mater. 3 (2016) 015005. doi:10.1088/2053-1583/3/1/015005.
- [42] R.F. Frindt, Single Crystals of MoS₂ Several Molecular Layers Thick, J. Appl. Phys. 37 (1966) 1928–1929. doi:10.1063/1.1708627.

Figures

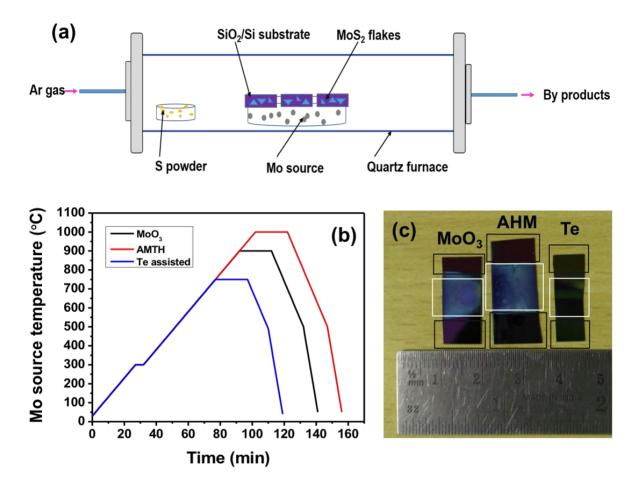


Fig. 1. (a) Schematic illustration of the inside view of the quartz tube of single zone mini CVD setup. (b) CVD temperature-time programme graph for different Mo precursors. (c) Image of asgrown MoS₂ samples on SiO₂/Si substrate showing large area growth. Black boxes represent regions of as-grown MoS₂ flakes while white boxes show MoO₂ and MoOS₂ grown regions

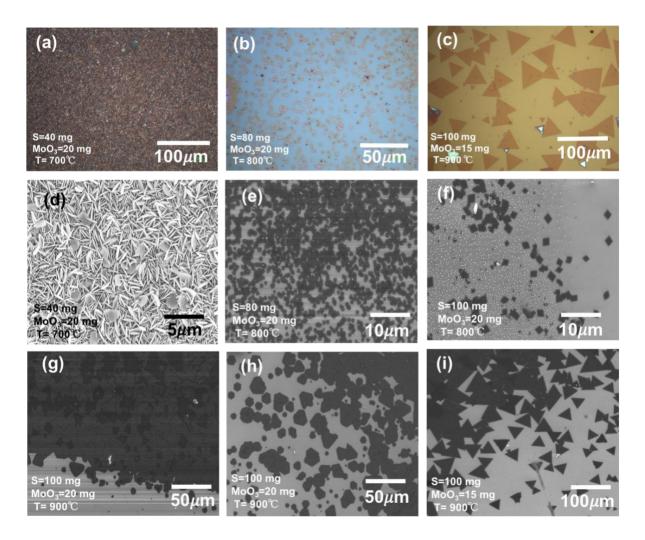


Fig. 2. Optical microscopy (OM) and scanning electron microscopy (SEM) images of different MoS₂ phase synthesised by MoO₃ as Mo source. (a) OM image of as-grown oxy-phase MoO₂, (b) MoOS₂, and (c) 1L-MoS₂, depicting the effect of precursors ratio and growth temperature on MoO₃. (d)-(i) SEM images of the evolution of MoS₂ from MoO₂ to highly crystalline 1L-MoS₂ flakes. Images (g) and (h) are captured at different locations of the same sample

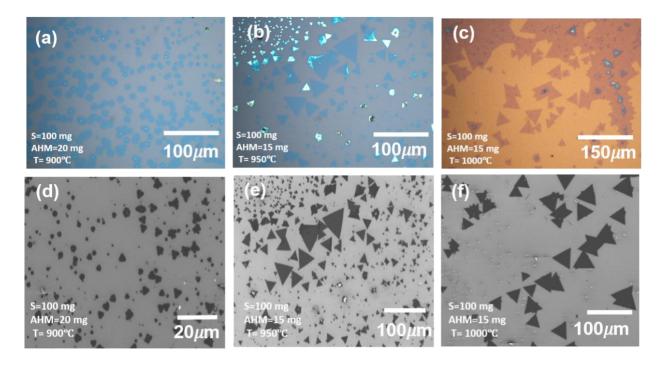


Fig. 3. Optical and SEM images representing different MoS₂ phases synthesised by AHM precursor as Mo source. (a) OM image of round shape oxy-phase MoS₂ micro-crystals acting as a nucleation centres for growth. (b) Bulk and 1L-MoS₂ flakes. (c) Large-sized crystalline uniform 1L-MoS₂ flakes. (d)-(f) SEM images corresponding to OM images showing the evolution of MoS₂ from MoO₂ to highly crystalline monolayer synthesised by AHM precursor as Mo source

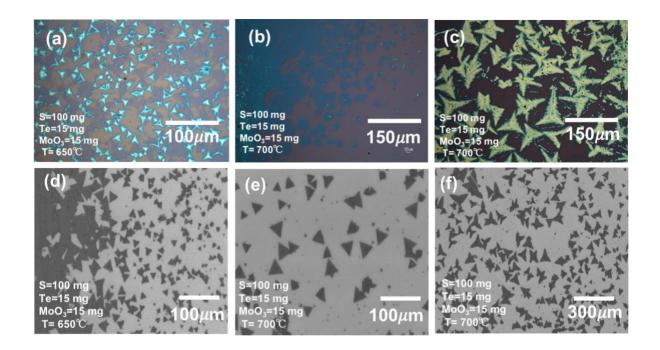


Fig. 4. Optical and SEM images of Te-assisted MoS₂ flakes. (a)-(c) optical micrographs and (d)-(f) are their corresponding SEM images of highly crystalline Te-assisted MoS₂ flakes

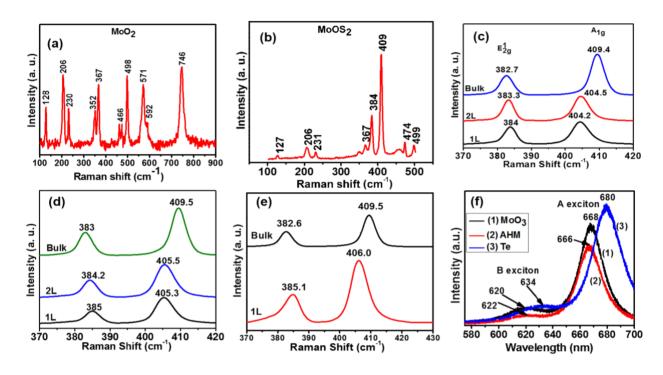


Fig. 5. Raman and photoluminescence measurements characterised by 532 nm laser. (a) and (b) Raman spectra of micro particles of MoO₂ and MoOS₂, respectively. (c) Raman spectrum of crystalline 1L, 2L, and bulk MoS₂ synthesised using MoO₃ precursor at 900°C. E_{12g} and A_{1g} Raman modes observed at 384 and 404.2 cm₋₁ (Δk =20.2 cm₋₁). (d) and (e) Raman spectra of CVD MoS₂ synthesised by AHM powder and Te-assisted growth, respectively. (f) PL spectrum of MoS₂ triangular MoS₂ flakes grown via a different combination of precursors. PL spectrum (1), (2), and (3) correspond to MoS₂ synthesised by MoO₃, AHM and Te assisted, respectively. In all these three PL spectrums, higher and lower energy peak corresponds to B exciton and A exciton, respectively

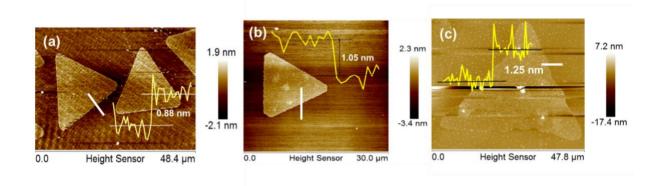


Fig. 6. AFM images and height profiles of as-grown MoS₂ flakes. AFM height profiles of corresponding AFM images are inserted in respective Fig. and white line in AFM images show the path of height profile measurements. (a) triangular crystalline, uniform 1L-MoS₂ synthesised using MoO₃ having a layer thickness of 0.88 nm. (b) crystalline truncated 1L-MoS₂ triangle of 1.05 nm grown by AHM. (c) Te-assisted pine shape triangular flake of 1L-MoS₂ (thickness ~1.25 nm) grown at lower temperature (750°C)